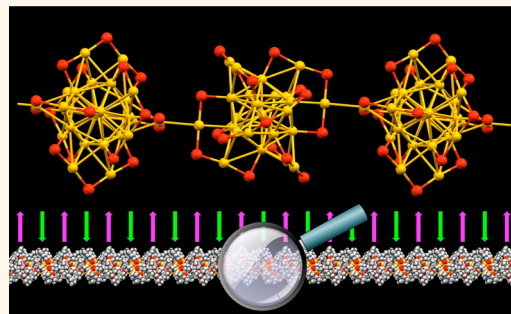


Gold Nanowired: A Linear $(\text{Au}_{25})_n$ Polymer from Au_{25} Molecular Clusters

Marco De Nardi,[†] Sabrina Antonello,[†] De-en Jiang,[‡] Fangfang Pan,[§] Kari Rissanen,[§] Marco Ruzzi,[†] Alfonso Venzo,^{†,‡} Alfonso Zoleo,[†] and Flavio Maran^{†,*}

[†]Department of Chemistry, University of Padova, Via Marzolo 1, 35131 Padova, Italy, [‡]Department of Chemistry, University of California, Riverside, California 92521, United States, [§]Department of Chemistry, Nanoscience Center, University of Jyväskylä, P.O. Box 35, 40014 Jyväskylä, Finland, and [‡]TENI-CNR c/o Department of Chemistry, University of Padova, Via Marzolo 1, 35131 Padova, Italy

ABSTRACT $\text{Au}_{25}(\text{SR})_{18}$ has provided fundamental insights into the properties of clusters protected by monolayers of thiolated ligands (SR). Because of its ultrasmall core, 1 nm, $\text{Au}_{25}(\text{SR})_{18}$ displays molecular behavior. We prepared a Au_{25} cluster capped by *n*-butanethiolates (SBu), obtained its structure by single-crystal X-ray crystallography, and studied its properties both experimentally and theoretically. Whereas in solution $\text{Au}_{25}(\text{SBu})_{18}^0$ is a paramagnetic molecule, in the crystal it becomes a linear polymer of Au_{25} clusters connected *via* single Au–Au bonds and stabilized by proper orientation of clusters and interdigitation of ligands. At low temperature, $[\text{Au}_{25}(\text{SBu})_{18}^0]_n$ has a nonmagnetic ground state and can be described as a one-dimensional antiferromagnetic system. These findings provide a breakthrough into the properties and possible solid-state applications of molecular gold nanowires.



KEYWORDS: gold nanoclusters · Au_{25} · polymer · X-ray crystallography · paramagnetism · antiferromagnetic coupling

Triggered by publication of the first structure of a thiolate-protected gold cluster,¹ the number of studies concerning properties^{2–3} and applications^{4–6} of gold clusters protected by monolayers of organic molecules (monolayer-protected clusters, MPCs) has increased dramatically. This is particularly true for MPCs displaying molecule-like properties (gold core diameter <1.5 nm), *i.e.*, systems where a sizable energy gap between the highest occupied molecular orbital (HOMO) and the lowest unoccupied MO (LUMO), a distinct electrochemical charging behavior, and molecular nuclear magnetic resonance (NMR) features are detected. Among these clusters, $\text{Au}_{25}(\text{SR})_{18}$ represents a true “gold mine” in the sense that it keeps furnishing an effective benchmark for gaining insights into properties of ultrasmall MPCs and developing and testing new concepts at the nanoscale.⁷ Solving the X-ray crystallography crystal structures of $\text{Au}_{102}(\text{SR})_{44}$,¹ $\text{Au}_{25}(\text{SR})_{18}$,^{8–11} and other MPCs^{12,13} has undoubtedly provided a sound nonspeculative basis for gaining a deep understanding of these systems and developing tools suitable to obtain information about the fine structure and the

electronic distribution of nanoclusters. The structure of $\text{Au}_{102}(\text{SR})_{44}$ showed how the surface Au atoms interact with thiolate ligands,¹ and a link with the corresponding self-assembled monolayers on extended gold surfaces^{14,15} could be established and discussed.¹⁶ This discovery elicited further research, notably to experimentally solve the structure of $\text{Au}_{25}(\text{SR})_{18}$ ^{8,9} and theoretically predict it.¹⁷ A remarkable example is the prediction of the structure of $\text{Au}_{38}(\text{SR})_{24}$,¹⁸ later assessed by X-ray crystallography.¹²

Such knowledge and successes have paved the way for developing new investigation methodologies and carrying out calculations aimed to predict possible structures. This is also the case of structures stabilized by multiple ligands, such as that of the biicosahedral Au cluster, in which two Au_{13} icosahedra share one vertex Au atom to form a sort of dimer consisting of 25 Au atoms, $[\text{Au}_{25}(\text{PPh}_3)_{10}(\text{SC}_2\text{H}_5)_5\text{Cl}_2]^{2+}$.¹⁹ This discovery triggered curiosity about the existence of possible MPC oligomers and even hypothetical polymers. First, a triicosahedral structure, $[\text{Au}_{37}(\text{Ph}_3)_{10}(\text{SCH}_3)_{10}\text{Cl}_2]^+$, was proposed.²⁰ Next, two MPC polymers or thiolated gold nanowires were suggested,²¹

* Address correspondence to flavio.maran@unipd.it.

Received for review June 9, 2014 and accepted August 3, 2014.

Published online August 03, 2014
10.1021/nn5031143

© 2014 American Chemical Society

one based on a vertex-sharing icosahedral Au_{13} chain where two neighboring icosahedra are further connected by five $-\text{SR}$ groups and another based on the face-sharing biicosahedral model and the $\text{RS}-\text{Au}-\text{SR}$ motifs, motivated by the structure of $\text{Au}_{38}(\text{SR})_{24}$.¹² A similar yet different dimeric structure was also solved, which is interestingly missing the shared vertex,²² and its electronic structure was analyzed from spherical harmonics analysis.²³

Despite the existing knowledge of structures and solution-phase properties of some MPCs, however, the physicochemical behavior of gold nanoclusters in the solid state is virtually unknown. Here we describe the discovery that whereas in solution Au_{25} protected by 18 *n*-butanethiolates (SBu) is a paramagnetic molecule, in the solid state it forms a linear polymer. Single-crystal X-ray crystallography analysis reveals that the Au_{25} polymer, hereafter indicated as $[\text{Au}_{25}(\text{SBu})_{18}^0]_n$, displays not only interesting features but also much less complicated structural motifs than addressed in theoretical studies: in particular, the clusters are connected by single $\text{Au}-\text{Au}$ bonds with no loss of atoms, and an important role of dispersion forces is inferred. This gold nanocluster polymer structure has not been observed previously in practice or predicted by theory. The properties of the polymer were studied both experimentally and theoretically, in comparison with the corresponding $\text{Au}_{25}(\text{SEt})_{18}$ cluster (Et = ethyl),¹¹ which despite its less hindered ligands remains monomeric under otherwise identical solid-state conditions. Analysis of its properties shows that polymer $[\text{Au}_{25}(\text{SBu})_{18}^0]_n$ is the thinnest gold nanowire ever described.

RESULTS AND DISCUSSION

Synthesis. The synthesis of $\text{Au}_{25}(\text{SBu})_{18}$ was carried out as recently described,²⁴ and full details are provided in the Supporting Information. Briefly, we prepared a solution of tetrachloroauric acid and tetraoctylammonium bromide in tetrahydrofuran and then added *n*-butanethiol to form a colorless solution of $\text{Au}(\text{I})$ -thiolate species. Addition of sodium borohydride followed by aging for 3 days yielded a solution displaying the typical UV-vis absorption spectrum of $\text{Au}_{25}(\text{SR})_{18}^-$ clusters. The as-prepared cluster is a diamagnetic anion. Its HOMO-LUMO gap determined from the onset of optical absorption in solution (Figure S1) is 1.35 eV. Similarly to $\text{Au}_{25}(\text{SC}_2\text{H}_4\text{Ph})_{18}^-$,²⁵ this estimate is in agreement with that obtained electrochemically, 1.30 eV, after correction of the relevant electrochemical formal potentials (E°) of peaks R1 and R2 for the charging energy (potential difference between O1 and R1: see Supporting Information). Quantitative one-electron oxidation of anion $\text{Au}_{25}(\text{SBu})_{18}^-$ to form the very stable, paramagnetic $\text{Au}_{25}(\text{SBu})_{18}^0$ cluster was performed by passage through a silica gel column under aerobic conditions,¹¹ as verified *via* characteristic changes observed in the UV-vis absorption spectrum (Figure S2). The

optical and electrochemical behaviors of $\text{Au}_{25}(\text{SBu})_{18}$ in solution are thus in line with those of other molecule-like $\text{Au}_{25}(\text{SR})_{18}$ clusters.²⁴

X-ray Crystallography. Crystals suitable for X-ray single-crystal diffraction experiment were obtained by slow crystallization at 4 °C of $\text{Au}_{25}(\text{SBu})_{18}^0$ dissolved in DCM in the presence of a tiny amount of acetonitrile, a solvent in which the cluster is insoluble. The asymmetric unit contains two halves of $\text{Au}-\text{Au}$ bonded $\text{Au}_{25}(\text{SBu})_{18}$ clusters. Each cluster has a centrosymmetric Au_{13} icosahedral core capped by six $-(\text{SBu})-\text{Au}-(\text{SBu})-\text{Au}-(\text{SBu})-$ half-crowns (Figures 1a and S3). The two MPCs have similar geometry and show no significant differences with respect to the other known thiolate-protected Au_{25} structures;^{8–11} the icosahedron's central Au atom is at the inversion center; 12 Au atoms interacting with the Au center form the icosahedron surface; six $\text{Au}_2(\text{SBu})_3$ half-crowns, hereafter indicated for simplicity as staples, cover the icosahedron *via* $\text{Au}-\text{Au}$ and $\text{S}-\text{Au}$ bonds. In terms of distances between the icosahedron and staple Au atoms, however, subtle differences are also detected, as detailed in the Supporting Information. These bond distances fall in the general range of aurophilic bond distances, generally regarded as ranging from *ca.* 2.9 to 3.5 Å, well below the van der Waals distance (3.80 Å).²⁶ Relevant bond distances are gathered in Table S1.

The striking feature of the $\text{Au}_{25}(\text{SBu})_{18}^0$ structure is the formation of a polymeric chain (Figure 1b) along the (111) lattice plane. The length of the $\text{Au}-\text{Au}$ bond linking two MPCs is 3.1518(9) Å, *i.e.*, a bond length larger than those in the Au_{13} core (2.78–2.97 Å) but still smaller than typical $\text{Au}_{\text{staple}}-\text{Au}_{\text{icosahedron}}$ bonds (3.17–3.18 Å). The torsional angle between the two connecting $\text{Au}-\text{Au}$ bonds on the opposite sides of each MPC is 180°, and this makes the polymer a precisely linear 1D chain. Interestingly, in one of the two staples involved in the bond between neighboring clusters, the longest distance between two Au atoms is observed, 3.369(10) Å (Figure 1a). We regard this pronounced elongation as the result of polymerization of the MPCs *via* one of the bonding atoms. We also note that for the two Au atoms forming the intercluster bond the $\text{S}-\text{Au}-\text{S}$ angle is almost straight, 177.3(2)° (MPC1) and 177.0(2)° (MPC2), whereas the $\text{S}-\text{Au}-\text{S}$ angle of the other staples is smaller, *ca.* 170°. Collectively, these distortions allow generating a 1D chain.

Because of some flexibility of the *n*-butyl chains, some SBu groups are disordered. For each staple of both $\text{Au}_{25}(\text{SBu})_{18}^0$ cluster types, the three alkyl groups are oriented in either an up-down-up or an up-up-down manner with respect to the $\text{S}(\text{R})-\text{Au}-\text{S}(\text{R})-\text{Au}-\text{S}(\text{R})$ plane, but not on the same side as found for one pair of staples in $\text{Au}_{25}(\text{SEt})_{18}^0$.¹¹ These results further confirm our previous conclusion that in the solid state the ligand type may affect the monolayer structure. It is worth noting that whereas $\text{Au}_{25}(\text{SBu})_{18}^0$

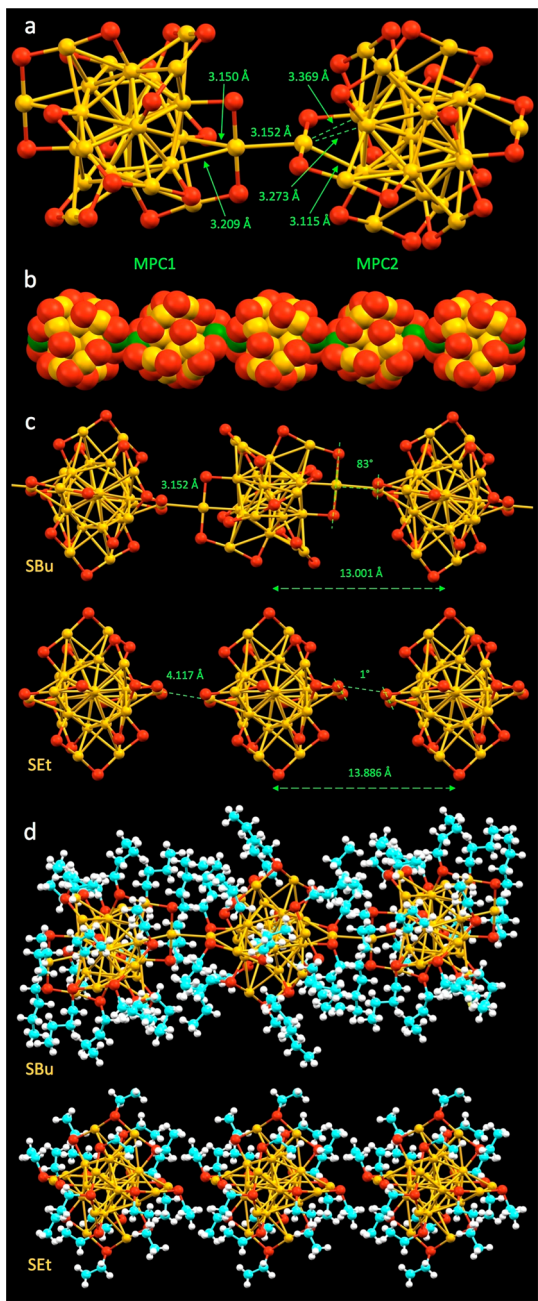


Figure 1. (a) Stick-and-ball view of the $\text{Au}_{25}(\text{S})_{18}$ skeletons of the two MPCs found in the $\text{Au}_{25}(\text{SBu})_{18}$ crystal. Au = yellow, S = red (in the first three panels, C and H atoms are removed for clarity). (b) View of the 1D chain evidenced along the (111) direction; connecting Au–Au bonds are in green. (c) Comparison between the $\text{Au}_{25}\text{S}_{18}$ skeletons of $\text{Au}_{25}(\text{SBu})_{18}$ and the $\text{Au}_{25}(\text{SEt})_{18}$ crystals, with relevant distances and torsional angles. (d) View of the two Au_{25} sequences to highlight interdigititation of ligands, in $\text{Au}_{25}(\text{SBu})_{18}$, or its absence, in $\text{Au}_{25}(\text{SEt})_{18}$. C = light blue, H = white.

forms a polymer, the “nearly naked” $\text{Au}_{25}(\text{SEt})_{18}^0$ does not. In fact, a striking difference between these two structures is the relative orientation of the two closest staples between neighboring clusters. Figure 1c shows that whereas in $\text{Au}_{25}(\text{SBu})_{18}^0$ the Au–Au bonded staples are oriented almost perpendicularly to each other (torsional angle 83°), which results in a distance

between two neighboring central Au atoms of only 13.001 \AA , in $\text{Au}_{25}(\text{SEt})_{18}^0$ the corresponding angle is *ca.* 1° and the distance 13.886 \AA . The interstaple Au–Au distance in $\text{Au}_{25}(\text{SEt})_{18}^0$ is thus clearly longer than in $\text{Au}_{25}(\text{SBu})_{18}^0$: $4.117 \text{ vs } 3.152 \text{ \AA}$. For $\text{Au}_{25}(\text{SC}_2\text{H}_4\text{Ph})_{18}^0$,¹² which is protected by bulkier ligands, the minimum distance between two central Au atoms is 16.412 \AA and that between two Au atoms of the closest staples is 6.969 \AA . These comparisons suggest that a “twist-and-lock” mechanism might be responsible for formation of the $[\text{Au}_{25}(\text{SBu})_{18}^0]_n$ polymer, where a *ca.* 90° twist allows for interdigititation (lock) of ligands having proper length. The latter feature is evidenced in Figure 1b, in comparison with $\text{Au}_{25}(\text{SEt})_{18}^0$, in which no interdigititation is observed. These observations would imply that too short (no lock) or too long ligands (steric hindrance hampering a sufficiently short intercluster Au–Au distance) are not suitable for stabilizing the 1D polymer. To estimate the driving force for such a twist-and-lock mechanism, we computed the binding energy between two $\text{Au}_{25}(\text{SBu})_{18}^0$ clusters in a dimeric state by dispersion-corrected density functional theory (DFT) and found it to be quite strong, at -2.25 eV . Without dispersion interactions, the binding energy diminishes to a much lower value, -0.28 eV . In other words, the lock is made possible by van der Waals interactions among SBu ligands of neighboring clusters. This “sticky” interaction between ligands thus appears to be essential for setting up ideal conditions for Au–Au bond formation. These Au–Au bonds are sufficiently strong to cause some local deformation of the staples involved. Formation of a linear chain but not a branched 3D polymer shows that both dispersion interactions and directional Au–Au bond formation concur to stabilize the observed structure.

NMR Analysis. The discovery that $\text{Au}_{25}(\text{SBu})_{18}^0$ is a paramagnetic monomer in solution but becomes a polymer in the solid state prompted us to carry out specific calculations and experiments aimed at understanding the fundamental properties of this new material. In $\text{Au}_{25}(\text{SR})_{18}$ clusters, the 18 thiolated ligands forming the monolayer split into a group of 12 inner ligands, in which sulfur makes bonds with one staple Au atom and one icosahedron Au atom, and a group of 6 outer ligands in which the bonds are only with staple Au atoms.⁸ The two groups of ligands display distinct NMR spectroscopy patterns, a difference that is magnified for some resonances when the cluster becomes paramagnetic.^{11,24,27} Figure 2 illustrates that the effect of the unpaired electron mostly concerns the methylene groups in positions α , β , and γ of the inner ligands and the α methylene of the outer ligands (*cf.* Figure 2). This NMR behavior is caused by the contact interaction of the nuclear magnetic moments with the unpaired electron and can be taken as a probe of whether the singly occupied MO (SOMO), and thus the spin density, spreads onto those specific nuclei. As a matter of fact,

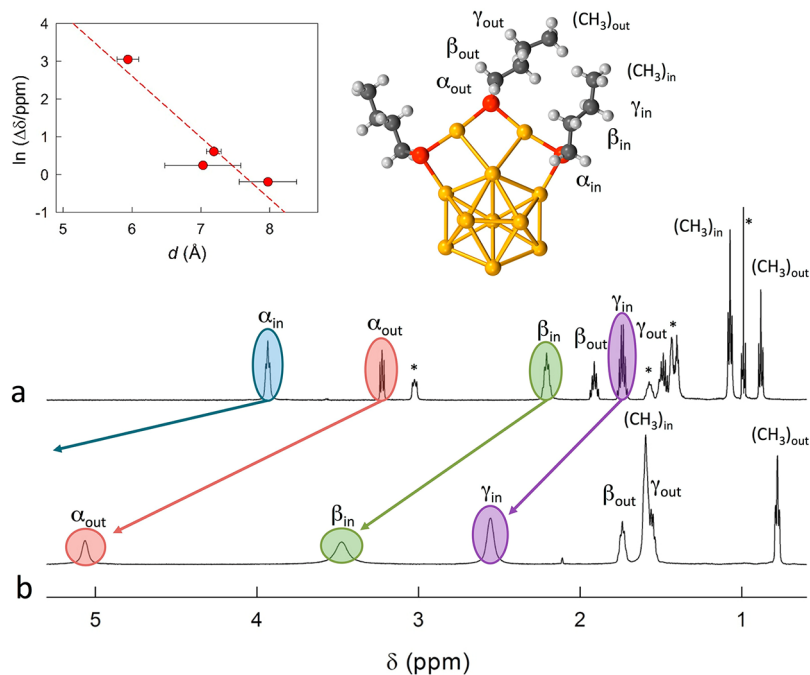


Figure 2. (a) ^1H NMR spectrum of $[n\text{-Oct}_4\text{N}^+][\text{Au}_{25}(\text{SBu})_{18}^-]$. The peaks marked with a star pertain to $n\text{-Oct}_4\text{N}^+$. (b) ^1H NMR spectrum of $\text{Au}_{25}(\text{SBu})_{18}^0$. Both samples were in benzene- d_6 at 25 $^\circ\text{C}$. Symbols α , β , and γ refer to the positions of inner and outer methylene groups from sulfur, as indicated in the structure (for clarity, only one staple is displayed). Arrows indicate the most significant shifts observed upon oxidation of $\text{Au}_{25}(\text{SBu})_{18}^-$ to $\text{Au}_{25}(\text{SBu})_{18}^0$. The $(\alpha\text{-CH}_2)_{\text{in}}$ resonance is at 25 ppm. Inset shows the resonance difference against the average distance of carbon atom of the corresponding CH_2 groups (of all staples of the two MPC types, with standard deviation error bars) from the icosahedron's central Au atom.

we have previously shown that specific DFT calculations could nicely reproduce the NMR spectrum of radical $\text{Au}_{25}(\text{SC}_2\text{H}_4\text{Ph})_{18}^0$ and that the spin density spans over the ligands' methylene groups.²⁷ Distance from the gold core is thus a crucial parameter. According to the X-ray structure, for $\text{Au}_{25}(\text{SBu})_{18}^0$ the distances from the central Au atom to the carbon atoms of the $(\alpha\text{-CH}_2)_{\text{in}}$, $(\beta\text{-CH}_2)_{\text{in}}$, $(\gamma\text{-CH}_2)_{\text{in}}$, and $(\alpha\text{-CH}_2)_{\text{out}}$ groups are 5.9(2), 7.0(6), 8.0(4), and 7.2(1) \AA , respectively. The MPC charge state does not significantly affect the $(\beta\text{-CH}_2)_{\text{out}}$ resonance, as this group is already quite distant, 8.1(2) \AA . Similar distance values are observed for $\text{Au}_{25}(\text{SEt})_{18}$ in the solid state:¹¹ $(\alpha\text{-CH}_2)_{\text{in}}$, 6.1(2); $(\beta\text{-CH}_3)_{\text{in}}$, 6.8(7); $(\alpha\text{-CH}_2)_{\text{out}}$, 7.2(1); $(\beta\text{-CH}_3)_{\text{out}}$, 8.1(1) \AA . In the $[\text{Au}_{25}(\text{SBu})_{18}^0]_n$ polymer, the midpoint distance between the central Au atoms of two neighboring clusters is only 6.5 \AA , and therefore, on the basis of the above resonance values, the SOMOs of neighboring clusters are expected to overlap quite significantly. DFT calculations of the orbitals of a $\text{Au}_{25}(\text{SBu})_{18}^0$ dimer, based on the crystallographic structure, provide support for this view, as illustrated in Figure S9. For $\text{Au}_{25}(\text{SEt})_{18}^0$, on the other hand, the average midpoint distance along the three crystallographic axes is distinctly larger, 7.0(1) \AA , which suggests a much reduced interaction. The case of the more hindered $\text{Au}_{25}(\text{SC}_2\text{H}_4\text{Ph})_{18}$ cluster, for which the minimum center-to-center half-distance in the crystal already is 8.2 \AA , points to a particularly pronounced lack of interaction.

DFT Calculations. An important question now arises about what happens when the SOMOs overlap. To shed light on this question and, more generally, the properties of polymer $[\text{Au}_{25}(\text{SBu})_{18}^0]_n$, we performed DFT calculations of the crystal with periodic boundary conditions, in comparison with the $\text{Au}_{25}(\text{SEt})_{18}^0$ and $\text{Au}_{25}(\text{SC}_2\text{H}_4\text{Ph})_{18}^0$ crystals for which the structures are known. In all three cases, calculations refer to the DFT-optimized structures obtained for $T = 0$ K by starting from the corresponding X-ray crystallographic structures, and the relative energies of the magnetic state (at one Bohr magneton per Au_{25} cluster) and the nonmagnetic state are compared. For $[\text{Au}_{25}(\text{SBu})_{18}^0]_n$, we found that in the crystal the cluster has a nonmagnetic ground state lower in energy than the magnetic state by 27 meV. This is in contrast to the situation arising for $\text{Au}_{25}(\text{SEt})_{18}^0$ and $\text{Au}_{25}(\text{SC}_2\text{H}_4\text{Ph})_{18}^0$ crystals in which the magnetic state now is lower in energy by 18 and 34 meV, respectively. A nonmagnetic ground state implies that the otherwise unpaired electron in the isolated $\text{Au}_{25}(\text{SBu})_{18}^0$ cluster is paired up in the ground state of the $\text{Au}_{25}(\text{SBu})_{18}^0$ crystal, leading to a fully occupied valence band (VB) and an empty conduction band (CB). Electron pairing is thus in agreement with the NMR prediction about the SOMOs' overlap. Concerning the $\text{Au}_{25}(\text{SEt})_{18}^0$ crystal, for which the room-temperature NMR behavior suggests a possible borderline behavior, calculations point to a magnetic ground state at 0 K, although less pronounced than for $\text{Au}_{25}(\text{SC}_2\text{H}_4\text{Ph})_{18}^0$. Figure 3a shows the density

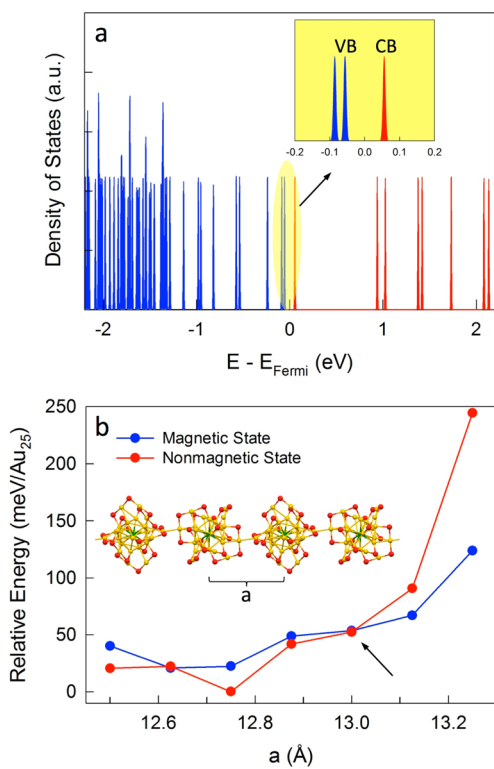


Figure 3. (a) Electronic density of states of the $\text{Au}_{25}(\text{SBu})_{18}$ crystal structure optimized further by density functional theory in the nonmagnetic state at 0 K. Inset shows a zoom-in of the region near the Fermi energy, with the valence band (VB) and conduction band (CB) labeled. (b) Relative energy of the nonmagnetic and magnetic states of the one-dimensional $\text{Au}_{25}(\text{SCH}_3)_{18}$ polymer as a function of the distance a between the central atoms of two neighboring clusters (Au = yellow, S = red, central Au = green, methyl groups removed for clarity). The arrow indicates the spin crossover. The experimental distances for SEt , SBu , and $\text{SC}_2\text{H}_4\text{Ph}$ are 13.886, 13.001, and 16.412 Å, respectively.

of states distribution and, particularly, that the nonmagnetic ground state of $[\text{Au}_{25}(\text{SBu})_{18}]_n^0$ has a band gap (energy difference between VB and CB) of *ca.* 0.12 eV at 0 K. Such a small energy gap suggests that at room temperature the $\text{Au}_{25}(\text{SBu})_{18}^0$ crystal should behave as a narrow-gap semiconductor.

The energetics of nonmagnetic vs magnetic states is closely related to the intercluster distance or the closest Au – Au contact. When there is no close contact between two neighboring Au_{25} clusters, the magnetic state is preferred. This is the case of $\text{Au}_{25}(\text{SEt})_{18}^0$ and, particularly, $\text{Au}_{25}(\text{SC}_2\text{H}_4\text{Ph})_{18}^0$. On the other hand, when a close contact occurs, the nonmagnetic state can be lower in energy than the magnetic state. To examine this spin crossover or the magnetic-to-nonmagnetic transition, we modeled a one-dimensional $[\text{Au}_{25}(\text{SCH}_3)_{18}]_n$ polymer as a function of the center-to-center distance between two neighboring Au_{25} clusters (Figure 3b). The polymer has the same structure of $[\text{Au}_{25}(\text{SBu})_{18}]_n^0$ and an intercluster Au – Au bond of 2.929 Å. As we stretch this polymer, which initially has a nonmagnetic ground state just like the $[\text{Au}_{25}(\text{SBu})_{18}]_n^0$

crystal (in this case, lower in energy by 22 meV and at an intercluster distance of 12.75 Å), both the magnetic and nonmagnetic states become higher in energy, but the nonmagnetic state has a higher rate of increase. At *ca.* 13.0 Å, the two states become almost degenerate in energy; after this crossover point, the magnetic state becomes lower in energy. Once again, these results support the view that a slightly more stable nonmagnetic state is expected for $\text{Au}_{25}(\text{SBu})_{18}^0$, whereas for $\text{Au}_{25}(\text{SEt})_{18}^0$ and especially $\text{Au}_{25}(\text{SC}_2\text{H}_4\text{Ph})_{18}^0$, which have longer intercluster distances, a magnetic state is predicted to be more stable. That a full transition occurs within less than 1 Å is particularly worth stressing and is in keeping with the outcome of the NMR analysis.

Electron Paramagnetic Resonance. A distinct advantage of starting from a well-defined paramagnetic cluster is the possibility of studying the system by electron paramagnetic resonance (EPR). EPR techniques detect the interactions between the resonating magnetic moment of a single paramagnetic center and its surroundings and thus provide fundamental information about the local field experienced by the paramagnetic centers and the hyperfine interactions caused by nearby magnetic nuclei.²⁸ For an assembly of paramagnets, magnetic moments are coupled together, directly or indirectly, by spin–spin dipolar and/or exchange interactions. Information about the mechanisms of interaction and the dynamics of the spin systems (relaxation effects) is obtained by analysis of the shape and width of EPR lines.²⁹ Continuous wave EPR (cw-EPR) and associated techniques have already proved to be very powerful tools for assessing the magnetic behavior of Au_{25} clusters^{30,31} and obtaining structural information.¹¹ We thus studied the cw-EPR behavior of the $[\text{Au}_{25}(\text{SBu})_{18}]_n^0$ crystals in comparison with the spectrum obtained for a glassy toluene solution. Figure 4a shows the two spectra, and the inset shows the same comparison after normalization for peak height. Figure 4b shows the corresponding spectra obtained for the closely related $\text{Au}_{25}(\text{SEt})_{18}^0$. The very different line width and the absence of a fine structure at 3000–4000 G for polymer $[\text{Au}_{25}(\text{SBu})_{18}]_n^0$ show that the physical state in which $\text{Au}_{25}(\text{SBu})_{18}^0$ is studied markedly affects the EPR signal. On the contrary, the spectra obtained for $\text{Au}_{25}(\text{SEt})_{18}^0$ in either physical state are very similar to each other and to that of $\text{Au}_{25}(\text{SBu})_{18}^0$ in frozen solution. More specifically, both clusters in frozen solution display the spectrum of a distribution of randomly oriented $S = 1/2$ spin-state molecules with anisotropic g -tensor components. The spectrum of $\text{Au}_{25}(\text{SBu})_{18}^0$ in frozen solution can thus be simulated very well (Figure S10), as already done for $\text{Au}_{25}(\text{SC}_2\text{H}_4\text{Ph})_{18}^0$ ^{30,31} using the same hyperfine coupling values and a very similar anisotropic g -tensor. Similar parameters can also be used for simulating the two spectra of $\text{Au}_{25}(\text{SEt})_{18}^0$. On the other hand, the spectrum of $[\text{Au}_{25}(\text{SBu})_{18}]_n^0$ cannot be simulated on the

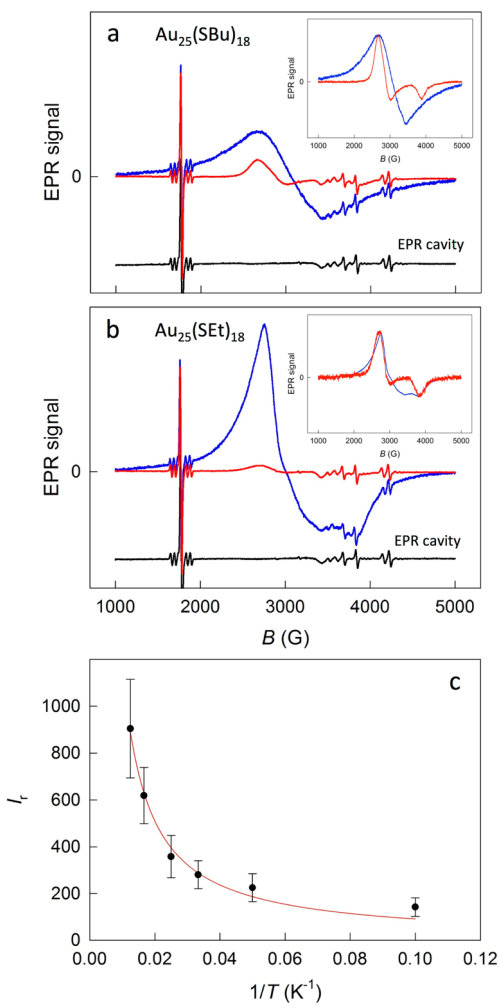


Figure 4. (a) Comparison between the cw-EPR spectra of solid (blue traces) and frozen toluene solution (red traces) of $\text{Au}_{25}(\text{SBu})_{18}$ at 20 K. The inset shows the same spectra but normalized for peak intensity. The black curve corresponds to the EPR cavity signal, subtracted in the inset for clarity. (b) Analogous comparison for $\text{Au}_{25}(\text{SEt})_{18}$ at 20 K. All spectra were obtained by using the following parameters: microwave frequency = 9.733 GHz; microwave power = 150 μW ; amplitude modulation = 1 G. (c) Bonner–Fisher–Hall fit to the experimental data, expressed as rescaled relative double-integrated EPR signal values ($r^2 = 0.985$).

basis of the same randomly oriented spin-state distribution model.

The cw-EPR spectrum of the $[\text{Au}_{25}(\text{SBu})_{18}]_n$ crystal differs from the other three spectra of Figure 4 in terms of both line shape and width of the signal. To shed light onto this aspect, the spectra of $[\text{Au}_{25}(\text{SBu})_{18}]_n$ were thus obtained at 10–80 K (Figure S11). The spectra show that as temperature increases, the line width increases rapidly, and this makes the EPR signal spread on a much wider magnetic-field range. On the basis of the crystallographic structure, we could successfully simulate the spectra by assuming a sequence of magnetic $S = 1/2$ centers interacting strongly along the polymer chain but weakly with those of other chains. Each magnetic center is viewed as experiencing an anisotropic magnetic interaction, resulting from

anisotropic dipolar and Heisenberg isotropic exchange couplings, with the spins of the two neighboring MPCs. For all temperatures employed, the simulations were optimized for shape by using an anisotropic g -tensor corresponding to that used for $\text{Au}_{25}(\text{SBu})_{18}^0$ in solution and a dipolar interaction of 650 MHz (for details, see the Supporting Information). The simulated EPR signals (cf. Figure S11) can be integrated to obtain the corresponding EPR absorption spectra. The latter are then further integrated to obtain the so-called double-integrated EPR signal (I_m). Our analysis shows that as T increases, whereas the EPR signal decreases as illustrated in Figure S11, I_m increases. This behavior is opposite of that observed for paramagnetic Au_{25} clusters in frozen solution, where an increase of T is accompanied by a decrease of I_m .³¹ I_m is proportional to the magnetic susceptibility of the sample (χ_m). Therefore, I_m values obtained at different temperatures provide an experimental estimate of the temperature dependence of χ_m . The problem of relating χ_m to temperature for a linear chain of $S = 1/2$ spins was originally solved by Bonner and Fisher,³² who computed the values of χ_m for the low-temperature limit when the coupling energy (J) is negative, *i.e.*, for antiferromagnetic coupling between neighboring spins. An isolated $[\text{Au}_{25}(\text{SBu})_{18}^0]_n$ chain represents an ideal one-dimensional antiferromagnetic system, and therefore, the Bonner and Fisher model should appropriately describe the temperature dependence of I_m and thus χ_m . We here define J as the energy difference between the nonmagnetic ground state and the higher energy magnetic state of $[\text{Au}_{25}(\text{SBu})_{18}^0]_n$. To estimate J from the values of I_m , we used the Hall expression:³³

$$\chi_m(T) = \frac{N_A g^2 \mu_B^2}{k_B T} \times \frac{0.25 + 0.074975x + 0.075235x^2}{1 + 0.9931x + 0.172135x^2 + 0.757825x^3} \quad (1)$$

where $x = |J/k_B T|$, N_A is the Avogadro number, μ_B is the Bohr magneton, and k_B is the Boltzmann constant.

Figure 4c shows that eq 1 provides a good fit ($r^2 = 0.985$) to properly rescaled I_m values (for details, see the Supporting Information). This analysis reveals two important aspects. First, the fact that the double-integrated EPR signal is an increasing function of T indicates that thermal activation makes a higher energy magnetic state more populated, thereby confirming the DFT prediction that the ground state of $[\text{Au}_{25}(\text{SBu})_{18}^0]_n$ is nonmagnetic. In other words, the EPR signal observed in the spectrum of polymer $[\text{Au}_{25}(\text{SBu})_{18}]_n$ is caused by the thermally induced population of the paramagnetic excited states and the recorded featureless, approximately Lorentzian, broad line results from the overlap of the signals due

to the paramagnetic excited states combined with a prevalently homogeneous line broadening due to the magnetic interactions between different centers. Second, a best fit to the experimental data yields a J value of 28(2) meV, *i.e.*, virtually identical to the DFT-calculated value of 27 meV. This outstanding agreement between EPR results and calculations thus provides compelling evidence that the $\text{Au}_{25}(\text{SBu})_{18}^0$ clusters self-organize into a linear $S = 1/2$ antiferromagnetic polymer chain.

CONCLUSIONS

$\text{Au}_{25}(\text{SBu})_{18}^0$ is a paramagnetic MPC that in solution displays the same molecule-like behavior of other Au_{25}

clusters. In the solid state, however, single-crystal X-ray crystallographic analysis reveals formation of a linear polymer composed by $\text{Au}_{25}(\text{SBu})_{18}^0$ units interconnected by single Au–Au bonds. A twist-and-lock mechanism between neighboring clusters and capping ligands appears to play an important role in polymer formation. This polymer structure has been neither observed nor predicted.³⁴ Full convergence of NMR, EPR, and DFT results indicates that the otherwise unpaired electrons of the $\text{Au}_{25}(\text{SBu})_{18}^0$ clusters pair up, with generation of a nonmagnetic ground state. We expect that these results will pave the way for exploring further physicochemical properties and possible applications at the nanoscale of this novel gold object.

EXPERIMENTAL SECTION

$\text{Au}_{25}(\text{SBu})_{18}$ was prepared as already described.²⁴ UV–vis, ^1H NMR (600 MHz), EPR, X-ray crystallography, and electrochemical instrumentation and general procedures have been described.^{11,24,27,31} Extensive details on synthesis and characterization of $\text{Au}_{25}(\text{SBu})_{18}$, ^1H NMR spectroscopy experiments, X-ray crystallographic analysis of $\text{Au}_{25}(\text{SBu})_{18}^0$ single crystals, computational analysis, and full description of EPR simulations and Bonner–Fisher analysis of $[\text{Au}_{25}(\text{SBu})_{18}^0]_n$ are provided in the Supporting Information. Additional figures include UV–vis absorption spectra and differential pulse voltammetry of $\text{Au}_{25}(\text{SBu})_{18}$ (Figures S1 and S2), structural details of the two MPCs forming $[\text{Au}_{25}(\text{SBu})_{18}^0]_n$, and views of the crystal along the a -, b -, and c -axes (Figures S3–S6), NMR spectra (Figures S7 and S8), orbital of the $\text{Au}_{25}(\text{SBu})_{18}$ dimer (Figure S9), cw-EPR spectra, and simulations of $[\text{Au}_{25}(\text{SBu})_{18}^0]_n$ and $\text{Au}_{25}(\text{SBu})_{18}$ in frozen solution (Figures S10 and S11). Table S1 gathers the Au–Au and S–Au bond lengths of the two MPCs forming the $[\text{Au}_{25}(\text{SBu})_{18}^0]_n$ polymer. The crystal structure of $\text{Au}_{25}(\text{SBu})_{18}^0$ and the corresponding checkCIF file have been deposited at the Cambridge Crystallographic Data Centre with CCDC number 998586, and the data can be obtained free of charge via www.ccdc.cam.ac.uk/data_request/cif.

Conflict of Interest: The authors declare no competing financial interest.

Acknowledgment. This work was financially supported by AIRC (FM, Project 12214: Innovative Tools for Cancer Risk Assessment and Early Diagnosis – 5 per mille), the Academy of Finland (KR, Grant Nos. 263256 and 265328), and (DJ) the U.S. Department of Energy, Office of Science, Basic Energy Sciences, Chemical Sciences, Geosciences, and Biosciences Division. This research used resources of the National Energy Research Scientific Computing Center (NERSC), which is supported by the Office of Science of the U.S. Department of Energy under Contract DE-AC02-05CH11231.

Supporting Information Available: Full details on the synthesis of $\text{Au}_{25}(\text{SBu})_{18}$ and NMR, EPR, DFT, and X-ray crystallography information. This material is available free of charge via the Internet at <http://pubs.acs.org>.

REFERENCES AND NOTES

- Jadzinsky, P. D.; Calero, G.; Ackerson, C. J.; Bushnell, D. A.; Kornberg, R. D. Structure of a Thiol Monolayer-Protected Gold Nanoparticle at 1.1 Å Resolution. *Science* **2007**, *318*, 430–433.
- Murray, R. W. Nanoelectrochemistry: Metal Nanoparticles, Nanoelectrodes, and Nanopores. *Chem. Rev.* **2008**, *108*, 2688–2720.
- Tsukuda, T. Toward an Atomic-Level Understanding of Size-Specific Properties of Protected and Stabilized Gold Clusters. *Bull. Chem. Soc. Jpn.* **2012**, *85*, 151–168.
- Negishi, Y.; Kurashige, W.; Niihoria, Y.; Nobusada, K. Toward the Creation of Stable, Functionalized Metal Clusters. *Phys. Chem. Chem. Phys.* **2013**, *15*, 18736–18751.
- Li, G.; Jin, R. Atomically Precise Gold Nanoclusters as New Model Catalysts. *Acc. Chem. Res.* **2013**, *46*, 1749–1758.
- Saha, K.; Agasti, S. S.; Kim, C.; Li, X.; Rotello, V. M. Gold Nanoparticles in Chemical and Biological Sensing. *Chem. Rev.* **2012**, *112*, 2739–2779.
- Parker, J. F.; Fields-Zinna, C. A.; Murray, R. W. The Story of a Monodisperse Gold Nanoparticle: $\text{Au}_{25}\text{L}_{18}$. *Acc. Chem. Res.* **2010**, *43*, 1289–1296.
- Heaven, M. W.; Dass, A.; White, P. S.; Holt, K. M.; Murray, R. W. Crystal Structure of the Gold Nanoparticle $[\text{N}(\text{C}_8\text{H}_7)_4][\text{Au}_{25}(\text{SCH}_2\text{CH}_2\text{Ph})_{18}]$. *J. Am. Chem. Soc.* **2008**, *130*, 3754–3755.
- Zhu, M.; Aikens, C. M.; Hollander, F. J.; Schatz, G. C.; Jin, R. Correlating the Crystal Structure of a Thiol-Protected Au_{25} Cluster and Optical Properties. *J. Am. Chem. Soc.* **2008**, *130*, 5883–5885.
- Zhu, M.; Eckenhoff, W. T.; Pintauer, T.; Jin, R. Conversion of Anionic $[\text{Au}_{25}(\text{SCH}_2\text{CH}_2\text{Ph})_{18}]^-$ Cluster to Charge Neutral Cluster via Air Oxidation. *J. Phys. Chem. C* **2008**, *112*, 14221–14224.
- Dainese, T.; Antonello, S.; Gascón, J. A.; Pan, F.; Perera, N. V.; Ruzzi, M.; Venzo, A.; Zoleo, A.; Rissanen, K.; Maran, F. $\text{Au}_{25}(\text{SEt})_{18}$, a Nearly Naked Thiolate-Protected Au_{25} Cluster: Structural Analysis by Single Crystal X-ray Crystallography and Electron Nuclear Double Resonance. *ACS Nano* **2014**, *8*, 3904–3912.
- Qian, H.; Eckenhoff, W. T.; Zhu, Y.; Pintauer, T.; Jin, R. Total Structure Determination of Thiolate-Protected Au_{38} Nanoparticles. *J. Am. Chem. Soc.* **2010**, *132*, 8280–8281.
- Zeng, C.; Qian, H.; Li, T.; Li, G.; Rosi, N. L.; Yoon, B.; Barnett, R. N.; Whetten, R. L.; Landman, U.; Jin, R. Total Structure and Electronic Properties of the Gold Nanocrystal $\text{Au}_{36}(\text{SR})_{24}$. *Angew. Chem., Int. Ed.* **2012**, *51*, 13114–13118.
- Maksymovych, P.; Sorescu, D. C.; Yates, J. T., Jr. Gold-Adatom-Mediated Bonding in Self-Assembled Short-Chain Alkanethiolate Species on the Au(111) Surface. *Phys. Rev. Lett.* **2006**, *97*, 146103.
- Cossaro, A.; Mazzarello, R.; Rousseau, R.; Casalis, L.; Verdini, A.; Kohlmeier, A.; Floreano, L.; Scandolo, S.; Morgante, A.; Klein, M. L.; *et al.* X-ray Diffraction and Computation Yield the Structure of Alkanethiols on Gold(111). *Science* **2008**, *321*, 943–946.
- Häkkinen, H. The Gold–Sulfur Interface at the Nanoscale. *Nat. Chem.* **2012**, *4*, 443–455.
- Acosta, J.; Walter, M.; Whetten, R. L.; Häkkinen, H.; Grönbeck, H. On the Structure of Thiolate-Protected Au_{25} . *J. Am. Chem. Soc.* **2008**, *130*, 3756–3757.

18. Pei, Y.; Gao, Y.; Zeng, X. C. Structural Prediction of Thiolate-Protected Au_{38} : A Face-Fused Bi-icosahedral Au Core. *J. Am. Chem. Soc.* **2008**, *130*, 7830–7832.
19. Shichibu, Y.; Negishi, Y.; Watanabe, T.; Chaki, N. K.; Kawaguchi, H.; Tsukuda, T. Biicosahedral Gold Clusters $[\text{Au}_{25}(\text{PPh}_3)_{10}(\text{SC}_n\text{H}_{2n+1})_5\text{Cl}_2]^{2+}$ ($n = 2–18$): A Stepping Stone to Cluster-Assembled Materials. *J. Phys. Chem. C* **2007**, *111*, 7845–7847.
20. Nobusada, K.; Iwasa, T. Oligomeric Gold Clusters with Vertex-Sharing Bi- and Triicosahedral Structures. *J. Phys. Chem. C* **2007**, *111*, 14279–14282.
21. Jiang, D. E.; Nobusada, K.; Luo, W. D.; Whetten, R. L. Thiolated Gold Nanowires: Metallic *versus* Semiconducting. *ACS Nano* **2009**, *3*, 2351–2357.
22. Das, A.; Li, T.; Nobusada, K.; Zeng, Q.; Rosi, N. L.; Jin, R. Total Structure and Optical Properties of a Phosphine/Thiolate-Protected Au_{24} Nanocluster. *J. Am. Chem. Soc.* **2012**, *134*, 20286–20289.
23. Goh, J.-Q.; Malola, S.; Häkkinen, H.; Akola, J. Role of the Central Gold Atom in Ligand-Protected Biicosahedral Au-24 and Au-25 Clusters. *J. Phys. Chem. C* **2013**, *117*, 22079–22086.
24. Antonello, S.; Arrigoni, G.; Dainese, T.; De Nardi, M.; Parisio, G.; Perotti, L.; René, A.; Venzo, A.; Maran, F. Electron Transfer through 3D Monolayers on Au_{25} Clusters. *ACS Nano* **2014**, *8*, 2788–2795.
25. Lee, D.; Donkers, R. L.; Wang, G.; Harper, A. S.; Murray, R. W. Electrochemistry and Optical Absorbance and Luminescence of Molecule-like Au_{38} Nanoparticles. *J. Am. Chem. Soc.* **2004**, *126*, 6193–6199.
26. Schmidbaur, H.; Schier, A. Auophilic Interactions as a Subject of Current Research: An Up-date. *Chem. Soc. Rev.* **2012**, *41*, 370–412.
27. Venzo, A.; Antonello, S.; Gascón, J. A.; Guryanov, I.; Leapman, R. D.; Perera, N. V.; Sousa, A.; Zamuner, M.; Zanella, A.; Maran, F. Effect of the Charge State ($z = -1, 0, +1$) on the Nuclear Magnetic Resonance of Monodisperse $\text{Au}_{25}[\text{S}(\text{CH}_2)_2\text{Ph}]_{18}^z$ Clusters. *Anal. Chem.* **2011**, *83*, 6355–6362.
28. Bennati, M.; Murphy, D. M. Electron Paramagnetic Resonance Spectra in the Solid State. In *Electron Paramagnetic Resonance—A Practitioner's Toolkit*, 1st ed.; Brustolon, M.; Giannello, M., Eds.; Wiley: Hoboken, NJ, 2009; pp 195–238.
29. Weil, J. A.; Bolton, J. R.; Wertz, J. E. *Electron Paramagnetic Resonance—Elementary Theory and Practical Applications*, 1st ed.; Wiley: Hoboken, NJ, 1994; pp 287–341.
30. Zhu, M.; Aikens, C. M.; Hendrich, M. P.; Gupta, R.; Qian, H.; Schatz, G. C.; Jin, R. Reversible Switching of Magnetism in Thiolate-Protected Au_{25} Superatoms. *J. Am. Chem. Soc.* **2009**, *131*, 2490–2492.
31. Antonello, S.; Perera, N. V.; Ruzzi, M.; Gascón, J. A.; Maran, F. Interplay of Charge State, Lability, and Magnetism in the Molecule-like $\text{Au}_{25}(\text{SR})_{18}$ Cluster. *J. Am. Chem. Soc.* **2013**, *135*, 15585–15594.
32. Bonner, J. C.; Fisher, M. E. Linear Magnetic Chains with Anisotropic Coupling. *Phys. Rev. A* **1964**, *135*, 640–658.
33. Hall, J. W. Ph.D. dissertation, University of North Carolina, Chapel Hill, 1977.
34. Jiang, D. The Expanding Universe of Thiolated Gold Nanoclusters and Beyond. *Nanoscale* **2013**, *5*, 7149–7160.